Journal of Electrical and Electronic Engineering
2022; 10(3): 121-127
http://www.sciencepublishinggroup.com/j/jeee
doi: 10.11648/j.jeee.20221003.17
ISSN: 2329-1613 (Print); ISSN: 2329-1605 (Online)

Possibility of Bending-Induced Fracture in Curved Double-Clad Fibers

Yoshito Shuto

Ofra Project, Iruma, Japan

Email address:
ofra@tuba.ocn.ne.jp

To cite this article:
Yoshito Shuto. Possibility of Bending-Induced Fracture in Curved Double-Clad Fibers. *Journal of Electrical and Electronic Engineering*. Vol. 10, No. 3, 2022, pp. 121-127. doi: 10.11648/j.jeee.20221003.17

Received: June 12, 2022; **Accepted**: June 24, 2022; **Published**: June 27, 2022

Abstract: Rare-earth-doped optical fibers are one of the most promising solid-state lasers. In these fiber lasers, a cladding-pumping scheme using large-mode-area double-clad fibers (DCFs) is utilized to increase the overall conversion efficiency of pumping light and to overcome the restriction owing to the onset of stimulated Raman scattering. On the other hand, it is extremely challenging to increase the fiber core size while retaining the excellent beam quality because fibers with large core size allow propagation of several higher-order modes (HOMs), except for the fundamental mode (FM). In order to suppress HOMs, DCFs are bent with a relatively small bend radius. For the bent DCFs, the fracture behavior, including delayed fracture, was investigated on the basis of the fracture mechanics concept. When a bent DCF is subjected to a high applied stress, failure occurs by the extension of a crack from the surface of the inner cladding (silica glass) layer of the DCF. When DCFs with core diameters of 20 and 40 μm were curved to be stored in the apparatus to maintain large bending radii of > 245 and 275 mm, respectively, it was found that both instantaneous and delayed fracture of bent DCFs could not occur in either air or distilled water. When a DCF is homogeneously curved in air and in water, bending loss occurs in the core and the optical power lost in the core is emitted from the outer interface (or boundary) between the inner cladding (silica glass) and outer cladding (low-index polymer) layers. As the transmittance of the polymer is not 100%, the leaked light is absorbed and heat accumulates in the polymer. The heat generated in the polymer through the absorption of optical power is transferred to the neighboring cladding (silica glass) layer. When the temperature of the outer wall of the cladding layer is higher than that of the inner wall, tensile stress is generated on the inner wall and compressive stress is generated on the outer wall. The thermal stress generated on the inner wall was estimated. It was concluded that the instantaneous fracture of curved DCFs could not occur in air or in distilled water under high-power laser operation.

Keywords: Double-Clad Fiber, Bending, Fracture Strength, Time to Failure, Fracture Mechanics

1. Introduction

Rare-earth-doped optical fibers are one of the most promising solid-state lasers for efficient diode-pumped high-power continuous-wave (CW) laser systems and fiber chirped-pulse amplification (CPA) systems. The output power from the ytterbium (Yb)-doped fiber lasers has abruptly increased over the past decade [1-6]. High conversion efficiencies from pump light are obtained in Yb-doped double-clad fibers (DCFs) by using a cladding-pumping scheme [7] to ensure that virtually all of the incident pump power is absorbed in the doped fiber core.

To overcome the restriction owing to the onset of stimulated Raman scattering (SRS), low-numerical-aperture (NA) large-mode-area (LMA) fibers [8] are utilized as DCFs. Typical LMA fibers used in the CW laser operation have core diameters of 20-40 μm and NA of < 0.09 [9-14]. A high output power of > 200 W in the CW laser operation using cladding-pumped Yb-doped and/or Nd+Yb-codoped LMA fibers [9-24] has been reported.

On the other hand, it is extremely challenging to increase the fiber core size while retaining an excellent beam quality because fibers with large core sizes allow propagation of several higher order mode (HOM), except for the fundamental mode (FM). In order to suppress HOMs, DCFs are bent with a relatively small bend radius [13, 14, 24].

It is well known that failures at bends in an optical fiber are caused by light leaking from the core when the fiber is

accidentally bent tightly with a high power input [25-33]. Two failure regimes have been classified by Sikora *et al.*, which they named regime 1 (R1) and regime 2 (R2) failures [27]. Among them, R1 failure will lead to the catastrophic failure of the fiber and the burning of the coating [28, 33]. In the previous paper [34], we clarified allowable curvature radii of the bent DCFs which were necessary to prevent the R1 failure and/or the generation of fiber fuse phenomenon under high-power laser operation.

The stress distribution in the straight DCF was studied by Brown and Hoffman to estimate the radially varying index of refraction due to the stress-optic effect [35]. They also calculated the maximum tolerable heat power per unit length using the tensile-limited stress for the DCF. Zervas investigated the power limiting factor of high-power fiber amplifiers using a failure-in-time analysis [36]. However, the possibility of fracture in the bent DCF is not clear at the moment. In this article, the fracture behavior, including delayed fracture, of the bent DCFs was investigated on the basis of the fracture mechanics concept.

2. Fracture Behavior in Curved DCF

When optical fibers are fabricated with the fiber drawing apparatus, it is very difficult to produce a long defect-free fiber. It should be noted that the existence of a small crack on the surface is always taken into account in the determination of the critical safe stress applicable to a fiber without breakage.

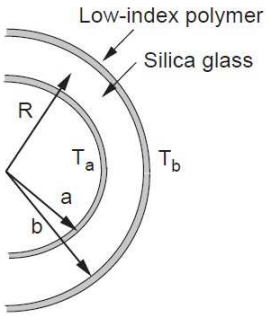

Figure 1. *Schematic of curved DCF.*

When a DCF is homogeneously curved with the bending radius R, as shown in Figure 1, tensile stress is generated on the outer wall ($r = b$) and a compressive stress is generated on the inner wall ($r = a$). Since most glass materials are more resistant to compression than to tension, it is expected that the surface of the outer wall will be susceptible to fracture owing to the presence of tensile stress.

The tensile stress at $r = b$ is given by

$$\sigma = \frac{E(b-R)}{R} \quad (1)$$

where E (= 73 GPa) is Young's modulus of the silica glass.

The relationships between R and σ in the bent DCF was investigated using Eq. (1). The calculated result is shown in Figure 2. In the calculation, the diameter ($2r_1$) of the inner cladding layer of the DCF was assumed to be 400 μm, which leads to b - R = 200 μm.

The inert strength σ_{IC} of 5,670 MPa has been reported for silica optical fibers [37]. As shown in Figure 2, σ decreases rapidly with increasing R and becomes smaller than σ_{IC} at R ≥ 3 mm. For R = 100-300 mm, the corresponding σ values are listed in Table 1.

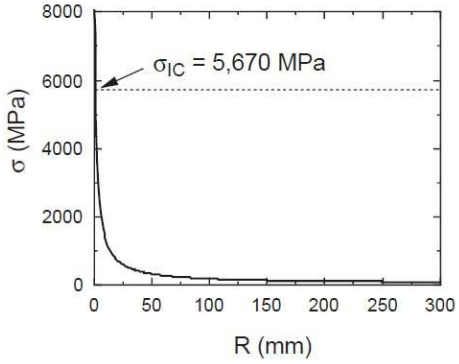

Figure 2. *Tensile stress on outer wall versus curvature radius in bent DCF.*

Table 1. *Tensile stress against curvature radius.*

R **(mm)**	**σ (MPa)**
100	146
150	97
200	73
250	58
300	49

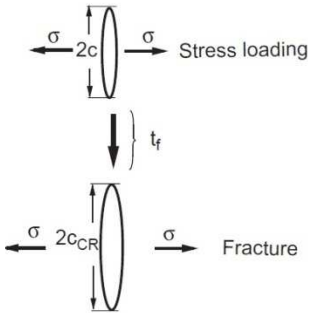

Figure 3. *Fracture in DCF.*

When a bent DCF is subjected to a high applied stress (σ), failure occurs by the extension of a crack from the surface of the inner cladding (silica glass) layer of the DCF. A crack with an initial size of $2c$ grows until it reaches a critical size $2c_{CR}$ after the passage of the time to failure t_f. When c becomes c_{CR}, the part of the cladding layer, in which the crack exists on the surface, fails almost instantaneously, as shown in Figure 3.

On the other hand, if the applied stress is reduced, a time delay is observed between the time of first exposure to stress and the time of failure. This phenomenon is called “delayed failure”.

In the following, the fracture for which t_f is very short (< 1 s), is referred to as “instantaneous fracture” in order to distinguish the fracture patterns.

In the next section, the fracture strength of the bent DCFs, which is an important parameter in the instantaneous fracture, is estimated.

3. Fracture Strength of Curved DCF

It is assumed that an internal crack (flaw) with a half-length of c exists on the fiber surface perpendicular to the fiber axis and c is fairly small compared with the fiber diameter.

The critical stress intensity factor K_{IC} at the crack front is approximately given by [38]

$$K_{IC} = \frac{2.2}{\sqrt{c}}\sigma_f\sqrt{c} \equiv Y\sigma_f\sqrt{c} \quad (2)$$

where Y is a geometric constant and σ_f is the tensile fracture strength acting on the fiber surface. The K_{IC} values of 0.75-0.87 MPa $m^{1/2}$ [38-41] have been reported for conventional optical fibers in air.

On the other hand, the water immersion of DCFs is performed to remove heat efficiently from the fiber surface [11]. K_{IC} for the fiber in distilled water is estimated to be about 0.37 MPa $m^{1/2}$ [38], which is about half that in air.

The relationships between c and σ_f in air and in distilled water were investigated using Eq. (2). The calculated results are shown in Figure 4. In the calculation, K_{IC} values of 0.75 and 0.37 MPa $m^{1/2}$ were used for the estimation of σ_f in air and in water, respectively. As shown in Figure 4, σ_f decreases rapidly with increasing c. For example, if a fiber contains a flaw with c of 10 μm on the surface, σ_f is estimated to be 191 MPa in air and 94 MPa in water.

On the other hand, the inert strength σ_{IC} (5,670 MPa) corresponds to σ_f in air when the flaw size c is about 0.01 μm.

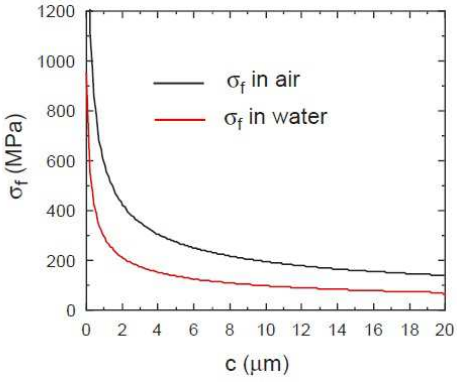

Figure 4. *Fracture strength in air and/or in distilled water versus half-length of flaw on fiber surface.*

For flaw size c = 1-20 μm, the corresponding σ_f values are listed in Table 2.

Table 2. *Fracture strength against flaw size.*

c (μm)	σ_f (MPa) in air	σ_f (Mpa) in water
1	604	298
2	427	211
5	270	133
10	191	94
15	156	77
20	135	67

As the typical crack size c of the conventional optical fiber is 1 μm or less [38] and the c of the glass is normally less than 10 μm [42], we can expect c on the inner cladding surface of the DCF to be slightly large (1-10 μm) compared with that of a conventional optical fiber. It was recommended for DCFs with core diameters of 20 and 40 μm being curved for storage in the apparatus to maintain large R values of > 245 and 275 mm, respectively, for high-power laser operation [34]. As shown in Table 1, tensile stresses of 50-60 MPa occur on the outer wall ($r = b$) when R is about 250-300 mm. These tensile stresses are smaller than the fracture strengths both in air and in water when c on the inner cladding surface of the DCF is 1-10 μm (see Table 2).

Therefore, it is concluded that when DCFs with core diameters of 20 and 40 μm are curved to be stored in the apparatus to maintain large R values of > 245 and 275 mm, respectively, instantaneous fracture does not occur in the bent DCFs.

In the next section, the time to failure, t_f, of the DCF is estimated, which is an important parameter in the delayed fracture.

4. Time to Failure of Curved DCF

The typical crack size c of the conventional optical fiber has a small value of 1 μm or less [38]. This was achieved by conducting a proof test [43, 44]. The samples of weaker fiber are eliminated during the proof test. The proof-test stress σ_p corresponds to the largest flaw size possible in the tested fiber, since any larger flaws would cause failure during the proof test.

On the other hand, the largest crack size on the inner cladding surface of the DCF is unknown, but it can be considered to be slightly large (1-10 μm), compared with that on a conventional optical fiber. Therefore, it was assumed that the fracture strength σ_f at c = 10 μm was used instead of σ_p in the estimation of the minimum time to failure, t_{min}, of the bent DCF.

For many glass and ceramic materials, the subcritical crack growth rate at a constant stress is described as a power function of the stress intensity factor K as [43, 45, 46]

$$\frac{dc}{dt} = AK^N, \quad (3)$$

where A and N are constants. It is well known that there is relationship between parameter A and the water vapor pressure [46] and the chemical interaction between strained crack-tip bonds in the silica glass and water molecules from the environment [47]. The subcritical crack growth process is thermally activated, and the existence of water molecules on the surface results in the lowering of the activation energy of this process [48]. As a result, the A value estimated in distilled water tends to be larger than that in air. Sawaki *et al*. found that the A value estimated in distilled water at 22°C was about 3.5 times that in air at 24°C [38].

t_{min} under a constant stress σ_a can be derived using the proof stress σ_p as [49]

$$t_{min} = B\sigma_a^{-N}\sigma_p^{N-2}, \quad (4)$$

where

$$B = \frac{2}{AY^2(N-2)K_{IC}^{N-2}}, \quad (5)$$

with K_{IC} being a critical stress intensity factor and Y a geometric constant.

The subcritical crack growth parameters N and B in air can be estimated to be 22.23 and 1.56×10^6 MPa^2 s, respectively, from dynamic fatigue tests of optical glass fibers [37]. In distilled water, B has been estimated to be 7.19×10^{11} MPa^2 s by using K_{IC} (= 0.37 MPa m$^{1/2}$) in water, which is about half that (0.75 MPa m$^{1/2}$) in air, and parameter A in water, which is about 3.5 times that in air [38].

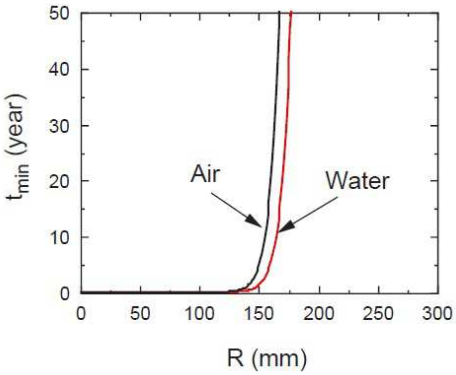

Figure 5. *Minimum time to failure in air and/or in distilled water versus curvature radius of bent DCF.*

The relationships between t_{min} and R in air and in distilled water were investigated using Eq. (1) and (4). The calculated results are shown in Figure 5. In the calculation, σ_p values of 191 and 94 MPa were used for the estimation of t_{min} in air and in water, respectively. As shown in Figure 5, the t_{min} values in air and in distilled water increase rapidly at $R > 150$ mm, and $t_{min} \geq 10$ years is obtained at $R \geq 173$ mm in air and $R \geq 184$ mm in distilled water.

Therefore, it is concluded that the delayed fracture of bent DCFs cannot occur in either air or distilled water when DCFs with core diameters of 20 and 40 μm are curved to be stored in the apparatus to maintain large R values of > 245 and 275 mm, respectively.

In the next section, the thermal stresses occurred in the bent DCFs are investigated in the case of temperature of the outer wall, T_b, being larger than that of the inner wall, T_a.

5. Thermal Stress in Curved DCF

When a DCF is homogeneously curved with the bending radius R, as shown in Figure 1, bending loss occurs in the core and the optical power lost in the core is emitted from the outer interface (or boundary) between the inner cladding (silica glass) and outer cladding (low-index polymer) layers [34]. As the transmittance of the polymer is not 100%, the leaked light is absorbed and heat accumulates in the polymer.

The heat generated in the low-index polymer through the absorption of optical power is transferred to the neighboring cladding (silica glass) layer, as shown in Figure 6.

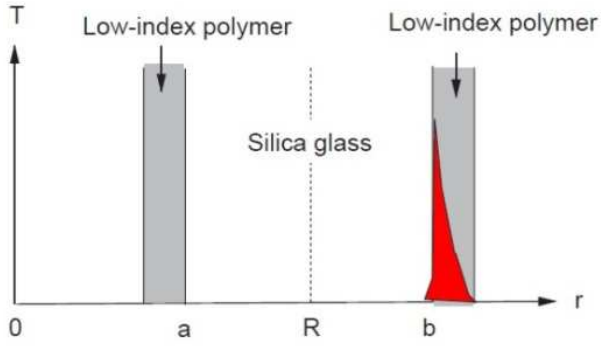

Figure 6. *Schematic of temperature distribution in curved DCF.*

A bent DCF can be modeled as a hollow disk, as shown in Figure 1, on the basis of the assumption that there is no temperature gradient in the plate thickness direction. When an axially symmetric temperature distribution $T = T(r)$ is given to the hollow silica glass disk, the radial thermal stress σ_r, the tangential thermal stress σ , and the axial (z) thermal stress σ_z are given as [50]

$$\sigma_r = \frac{\alpha E}{r^2}\left[\frac{r^2-a^2}{b^2-a^2}\int_a^b Trdr - \int_a^r Trdr\right], \quad (6)$$

$$\sigma_\varphi = \frac{\alpha E}{r^2}\left[\frac{r^2+a^2}{b^2-a^2}\int_a^b Trdr + \int_a^r Trdr - Tr^2\right], \quad (7)$$

$$\sigma_z = 0, \quad (8)$$

where it is assumed that the axial end faces are free of traction. In Eq. (6) and (7), (= 0.55×10^{-6} K^{-1} [39]) is the thermal expansion coefficient of the silica glass.

The temperature distribution for steady heat conduction is given by

$$T = T_a + (T_b - T_a)\ \ln(r/a) \ / \ \ln(b/a). \quad (9)$$

Substituting Eq. (9) into Eq. (6) and (7), the steady thermal stresses of the bent DCF become the following equations:

$$\sigma_r = \frac{\alpha E(T_a-T_b)}{2ln(b/a)}\left[-ln\left(\frac{b}{r}\right) + \frac{a^2}{b^2-a^2}\left(\frac{b^2}{r^2}-1\right)ln(b/a))\right], \quad (10)$$

$$\sigma_\varphi = \frac{\alpha E(T_a-T_b)}{2ln(b/a)}\left[1 - ln\left(\frac{b}{r}\right) - \frac{a^2}{b^2-a^2}\left(\frac{b^2}{r^2}+1\right)ln(b/a)\right]. \quad (11)$$

The thermal stresses generated on the inner ($r = a$) and outer ($r = b$) walls are given by the following equations:

$$(\sigma_r)_{r=a} = (\sigma_r)_{r=b} = 0, \quad (12)$$

$$(\sigma_\varphi)_{r=a} = \frac{\alpha E(T_b-T_a)}{2}\left[\frac{2b^2}{b^2-a^2} - \frac{1}{ln(b/a)}\right], \quad (13)$$

$$(\sigma_\varphi)_{r=b} = \frac{\alpha E(T_a-T_b)}{2}\left[-\frac{2a^2}{b^2-a^2} + \frac{1}{ln(b/a)}\right]. \quad (14)$$

When a DCF with an inner cladding radius r_1 of 200 μm is homogeneously curved with the bending radius R, a and b are given by R-200 μm and R+200 μm, respectively. In this case, the following approximation is valid for $R > 5$ mm.

$$\left[\frac{2b^2}{b^2-a^2} - \frac{1}{ln(b/a)}\right] \simeq \left[-\frac{2a^2}{b^2-a^2} + \frac{1}{ln(b/a)}\right] \simeq 1. \quad (15)$$

When the temperature of the outer wall ($r = b$) is higher than that of the inner wall ($r = a$), as shown in Figure 6, tensile stress is generated on the inner wall and compressive stress is generated on the outer wall.

As described above, when a DCF is homogeneously curved with the bending radius R, tensile stress is generated on the outer wall ($r = b$) and compressive stress is generated on the inner wall ($r = a$). Therefore, the thermally induced tensile stress at the inner wall is lowered by the bending-induced compressive stress. The tensile stress generated on the inner wall ($r = a$) is given by the following equation:

$$\left(\sigma_{\varphi}\right)_{r=a} \approx \frac{\alpha E(T_b - T_a)}{2} + \frac{E(a-R)}{R} \quad (16)$$

The relationships between $\left(\sigma_{\varphi}\right)_{r=a}$ and T_b of the bent DCF on the cases of R = 200 and 300 mm were investigated using Eq. (16). The calculated results are shown in Figure 7.

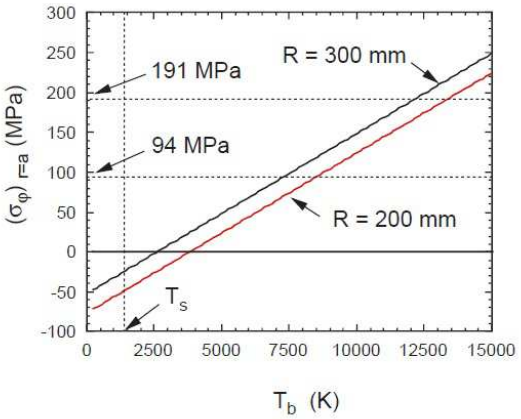

Figure 7. *Tensile stress at inner wall versus temperature of outer wall in bent DCF.*

As shown in Figure 7, $\left(\sigma_{\varphi}\right)_{r=a}$ increases with increasing T_b.

The values of 191 and 94 MPa are the fracture strengths in air and in water at c = 10 μm, as shown in Table 2. $\left(\sigma_{\varphi}\right)_{r=a}$ goes up to 191 MPa when T_b becomes 12,240 K or 13,450 K at R = 300 or 200 mm, respectively. Similarly $\left(\sigma_{\varphi}\right)_{r=a}$ goes up to 94 MPa when T_b becomes 7,400 K or 8,620 K at R = 300 or 200 mm, respectively.

These temperatures of 7,400-13,450 K are extremely high compared with the softening temperature T_s (= 1,373 K [27, 28]) of the silica glass. When the temperature at the heating part ($r = b$) of the silica glass exceeds T_s, the glass at the heating part will begin to deform and the compressive stress at this part will relax and disappear. The tensile stress at $r = a$ will be inhibited from increasing when T_b reaches T_s.

The values of $\left(\sigma_{\varphi}\right)_{r=a}$ at $T_b = T_s$ are about -27 and -51 MPa at R = 300 and 200 mm, respectively (see Figure 7). These are compressive stresses, not tensile stresses.

It was recommended for DCFs with core diameters of 20 and 40 μm being curved for storage in the apparatus to maintain large R values of > 245 and 275 mm, respectively, for high-power laser operation [34]. As described above, no tensile stresses occur on the inner wall ($r = a$) when R is 200-300 mm.

Instantaneous fracture occurs due to the tensile stresses larger than the fracture strengths both in air and in water when c on the inner cladding surface of the DCF is 1-10 μm.

Therefore, it is concluded that when DCFs with core diameters of 20 and 40 μm are curved to be stored in the apparatus to maintain large R values of > 245 and 275 mm, respectively, instantaneous fracture does not occur in air or in distilled water under high-power laser operation.

6. Conclusion

For the bent DCFs, the fracture behavior, including delayed fracture, was investigated on the basis of the fracture mechanics concept. When a bent DCF was subjected to a high applied stress, failure occured by the extension of a crack from the surface of the inner cladding (silica glass) layer of the DCF. When DCFs with core diameters of 20 and 40 μm were curved to be stored in the apparatus to maintain large bending radii of > 245 and 275 mm, respectively, it was found that both instantaneous and delayed fracture of bent DCFs could not occur in either air or distilled water. When a DCF is homogeneously curved in air and in water, bending loss occurs in the core and the optical power lost in the core is emitted from the outer interface (or boundary) between the inner cladding (silica glass) and outer cladding (low-index polymer) layers. As the transmittance of the polymer is not 100%, the leaked light is absorbed and heat accumulates in the polymer. The heat generated in the polymer through the absorption of optical power is transferred to the neighboring cladding (silica glass) layer. When the temperature of the outer wall of the cladding layer is higher than that of the inner wall, tensile stress is generated on the inner wall and compressive stress is generated on the outer wall. These thermal stress generated on the inner wall was estimated. It was concluded that the instantaneous fracture of curved DCFs could not occur in air or in distilled water under high-power laser operation up to 10 kW.

References

[1] Richardson D. J., Nilsson J., and Clarkson W. A. (2010). High power fiber lasers: current status and future perspectives. J. Opt. Soc. Am. B, 27 (11), B63-B92.

[2] Tünnermann A., Schreiber T., and Limpert J. (2010). Fibre lasers and amplifiers: an ultrafast performance evolution. Appl. Opt., 49 (25), F71-F78.

[3] Jauregui C., Limpert J., and Tünnermann A. (2013). High-power fibre lasers. Nat. Photonics, 7, 861-867.

[4] Fermann M. E. and Hartl I. (2013). Ultrafast fibre lasers. Nat. Photonics, 7, 868-874.

[5] Zervas M. N. and Codemand C. A. (2014). High power fiber lasers: a review. IEEE J. Selected Topics Quantum Electron., 20 (5), 0904123.

[6] Shi W., Fang Q., Zhu X., Norwood R. A., and Peyghambarian N. (2014). Fiber lasers and their applications. Appl. Opt., 53 (28), 6554-6568.

[7] Snitzer E., Po H., Hakimi F., Tumminelli R., and McCollum B. C. (1988). Double clad, offset core Nd fiber laser. Conf. on Optical Fiber Sensors, PD5-1.

[8] Broderick N. G. R., Offerhaus H. L., Richardson D. J., Sammut R. A., Caplen J., and Dong L. (1999). Large mode area fibers for high power applications. Opt. Fiber Technol., 5, 185-196.

[9] Jeong Y., Sahu J. K., Williams R. B., Richardson D. J., Furusawa K., and Nilsson J. (2003). Ytterbium-doped large-core fibre laser with 272 W output power. Electron. Lett., 39 (13), 977-978.

[10] Limpert J., Liem A., Zellmer H., and Tünnerman A. (2003). 500 W continuous-wave fibre laser with excellent beam quality. Electron. Lett., 39 (8), 645-647.

[11] Liu C.-H., Ehlers B., Doerfel F., Heinemann S., Carter A., Tankala K., Farroni J., and Galvanauskas A. (2004). 810 W continuous-wave and single-transverse-mode fibre laser using 20 μm core Yb-doped double-clad fibre. Electron. Lett., 40 (23), 1471-1472.

[12] Jeong Y., Sahu J. K., Payne D. N., and Nilsson J. (2004). Ytterbium-doped large-core fibre laser with 1 kW of continuous-wave output power. Electron. Lett., 40 (8), 470-471.

[13] Jeong Y., Sahu J. K., Payne D. N., and Nilsson J. (2004). Ytterbium-doped large-core fiber laser with 1.36 kW continuous-wave output power. Opt. Express, 12 (25), 6088-6092.

[14] Jeong Y., Boyland A. J., Sahu J. K., Chung S., Nilsson J., and Payne D. N. (2009). Multi-kilowatt single-mode ytterbium-doped large-core fiber laser. J. Opt. Soc. Korea, 13 (4), 416-422.

[15] Huang L., Wang W., Leng J., Guo S., Xu X., and Cheng X. (2014). Experimental investigation on evolution of the beam quality in a 2-kW high power fiber amplifier. IEEE Photon. Technol. Lett., 26 (1), 33-36.

[16] Khitrov V., Minelly J. D., Tumminelli R., Petit V., and Pooler E. S. (2014). 3 kW single-mode direct diode-pumped fiber laser. Proc. Soc. Photo-Opt. Instrum. Eng., 8961, 89610V-1-89610V-6.

[17] Yu H., Zhang H., Lv H., Wang X., Leng J., Xiao H., Guo S., Zhou P., Xu X., and Chen J. (2015). 3.15 kW direct diode-pumped near diffraction-limited all-fiber-integrated fiber laser. Appl. Opt., 54 (14), 4556-4560.

[18] Beier F., Hupel C., Kuhn S., Hein S., Nold J., Proske F., Sattler B., Liem A., Jauregui C., Limpert J., Haarlammert N., Schreiber T., Eberhardt R., and Tünnermann A. (2017). Single mode 4.3 kW output power from a diode-pumped Yb-doped fiber amplifier. Opt. Express, 25 (13), 14892-14899.

[19] Su R., Tao R., Wang X., Zhang H., Ma P., Zhao P., and Xu X. (2017). 3.7 kW monolithic narrow linewidth single mode fiber laser through simultaneously suppressing nonlinear effects and mode instability. Laser Phys. Lett., 14, 085102.

[20] Wang Y., Gao C., Tang X., Zhan H., Peng K., Ni L., Liu S., Li Y., Guo C., Wang X., Zhang L., Yu J., Jiang L., Lin H., Wang J., Jing F., and Lin A. (2018). 30/900 Yb-doped aluminophosphosilicate fiber presenting 6.85-kW laser output pumped with commercial 976-nm laser diodes. IEEE J. Lightwave Technol., 36 (16), 3396-3402.

[21] Xiao Q., Li D., Huang Y., Wang X., Wang Z., Tian J., Yan P., and Gong M. (2018). Directly diode and bi-directional pumping 6 kW continuous-wave all-fibre laser. Laser Phys., 28, 125107.

[22] Shima K., Ikoma S., Uchiyama K., Takubo Y., Kashiwagi M., and Tanaka D. (2018). 5-kW single stage all-fiber Yb-doped single-mode fiber laser for material processing. Proc. Soc. Photo-Opt. Instrum. Eng., 10512, 105120C-1-105120C-6.

[23] Ye Y., Yang B., Wang P., Zeng L., Xi X., Shi C., Zhang H., Wang X., Zhou P., and Xu X. (2021). Industrial 6 kW high-stability single-stage all-fiber laser oscillator based on conventional large mode area ytterbium-doped fiber. Laser Phys., 31, 035104.

[24] Fini J. M. (2006). Bend-resistant design of conventional and microstructure fibers with very large mode area. Opt. Express, 14 (1), 69-81.

[25] Percival R. M., Sikora E. S. R., and Wyatt R. (2000). Catastrophic damage and accelerated aging in bent fibres caused by high optical powers. Electron. Lett., 36 (5), 414-415.

[26] Logunov S. L. and DeRosa M. E. (2003). Effect of coating heating by high power in optical fibres at small bend diameters. Electron. Lett., 39 (12), 897-898.

[27] Sikora E. S. R., McCartney D. J., Farrow K., and Davey R. (2003). Reduction in fibre reliability due to high optical power. Electron. Lett., 39 (14), 1043-1044.

[28] Glaesemann G. S., Chien C., Clark D. A., Coon J., DeMartino S. E. and Logunov S. L. (2004). Analysis of optical fiber failures under bending and high power. Proc. Soc. Photo-Opt. Instrum. Eng., 5465, 1-10.

[29] Davis I. M., Glaesemann G. S., Ten S., and Winningham M. J. (2005). Optical fibres resilient to failure in bending under high power. Proc. European Conf. Opt. Commun. (ECOC 2005), We. 3.4.5, 471-472.

[30] Bigot-Astruc M., Sillard P., Gauchard S., Le Roux P., and Brandon E. (2006). Analysis of coating temperature increase in fibers under high power and tight bending. Proc. Opt. Fiber Commun. Conf. (OFC 2006), OFK4.

[31] Sikora E. S. R., McCartney D. J., and Wright J. V. (2007). Impact of coating ageing on susceptibility to high-power damage at fibre bends. Electron. Lett., 43 (4), 208-210.

[32] Logunov S. L., Chien C.-K., and Clark D. A. (2009). High power laser damage of standard and bent resistant fibres. Electron. Lett., 45 (20), 1019-1020.

[33] Kurokawa K. (2012). Optical fiber for high-power optical communication. Crystals, 2, 1382-1392.

[34] Shuto Y. (2022). Bending induced temperature increases in double-clad fibers for high-power fiber lasers. J. Electrical Electronics Eng., 10 (2), 64-70.

[35] Brown D. C. and Hoffman H. J. (2001). Thermal, stress, and thermo-optic effects in high average power double-clad silica fiber lasers. IEEE J. Quantum Electron., 37 (2), 207-217.

[36] Zervas M. N. (2012). Power scaling limits in high power fiber amplifiers due to transverse mode instability, thermal lensing and fiber mechanical reliability. Proc. Soc. Photo-Opt. Instrum. Eng., 10512, 1051205-1-1051205-5.

[37] Ritter J. E., Sullivan, Jr. J. M., and Jakus K. (1978). Application of fracture-mechanics theory to fatigue failure of optical glass fibers. J. Appl. Phys., 49 (9), 4779-4782.

[38] Sawaki Y., Sakaguchi S., Abe Y., and Kawasaki T. (1982). Fail safe design for optical fibers and cable units based on fracture mechanics. Trans. IECE Japan, E65 (6), 310-317.

[39] Krupke W. F., Shinn M. D., Marion J. E., Caird J. A., and Stokowski S. E. (1986). Spectroscopic, optical, and thermomechanical properties of neodymium- and chromium-doped gadolinium scandium gallium garnet. J. Opt. Soc. Am. B, 3 (1), 102-114.

[40] Kuester E. and Chang D. C. (1975). Surface-wave radiation loss from curved dielectric slabs and fibers. IEEE J. Quantum Electron., QE-11 (11), 903-907.

[41] Wiederhorn S. M. (1969). Fracture surface energy of glass. J. Am. Ceramic Soc., 52 (2), 99-105.

[42] Wiederhorn S. M. and Bolz L. H. (1970). Stress corrosion and static fatigue of glass. J. Am. Ceramic Soc., 53 (10), 543-548.

[43] Evans A. G. and Wiederhorn S. M. (1974). Proof testing of ceramic materials-an analytical basis for failure prediction. Int. J. Fracture, 10 (3), 379-392.

[44] Mitsunaga Y., Katsuyama Y., Kobayashi H., and Ishida Y. (1982). Failure prediction for long length optical fiber based on proof testing. J. Appl. Phys., 53 (7), 4847-4853.

[45] Evans A. G. (1972). A method for evaluating the time-dependent failure characteristics of brittle materials - and its application to polycrystalline alumina. J. Materials Sci., 7, 1137-1146.

[46] Sakaguchi S. and Kimura T. (1981). Influence of temperature and humidity on dynamic fatigue of optical fibers. J. Am. Ceramic Soc., 64 (5), 259-262.

[47] Michalske T. A. and Freiman S. W. (1983). A molecular mechanism for stress corrosion in vitreous silica. J. Am. Ceramic Soc., 66 (4), 284-288.

[48] Freiman S. W., Wiederhorn S. M., and Mecholsky, Jr. J. J. (2009). Environmentally enhanced fracture of glass: a historical perspective. J. Am. Ceramic Soc., 92 (7), 1371-1382.

[49] Ritter J. E. and Meisel J. A. (1976). Strength and failure predictions for glass and ceramics. J. Am. Ceramic Soc., 59 (11-12), 478-481.

[50] Takeuchi Y. and Noda N. (1989). Analysis of Thermal Stresses, 4th Ed., Chap. 5, Nissin Publishing Co., Ltd., Tokyo.